Journal of Materials Chemistry C

Accepted Manuscript

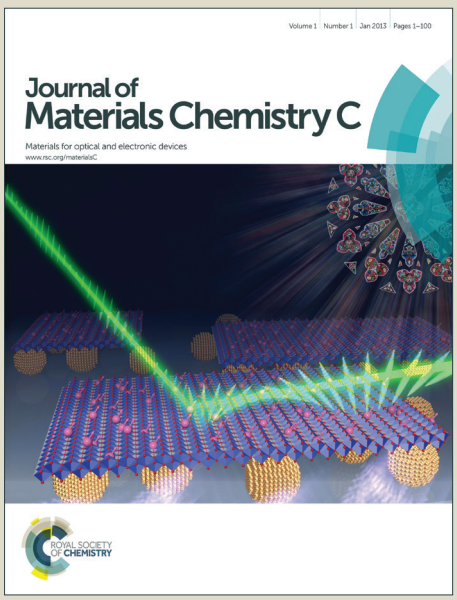

ROYAL SOCIETY OF CHEMISTRY

www.rsc.org/materialsC

Journal of Materials Chemistry C RSCPublishing

ARTICLE

Spatial degradation mapping and componentwise degradation tracking in polymer-fullerene blends

Cite this: DOI: 10.1039/x0xx00000x

E. B. L. Pedersen,[a] T. Tromholt,[a] Morten V. Madsen,[a] A. P. L. Böttiger,[a] M. Weigand,[b] F. C. Krebs[a] and J. W. Andreasen[a] ,

Received 00th January 2012,
Accepted 00th January 2012

DOI: 10.1039/x0xx00000x

www.rsc.org/

Using X-ray absorption the effects of photo degradation in active layer materials for polymer solar cells is investigated. Through observation of changes in the X-ray absorption energy spectra the degradation of the individual components is tracked in blends of poly-3-hexyl-thiophene (P3HT) and C60 butyric acid methyl ester (PCBM). The degradation rates in the blend are decreased by a factor of 3 for P3HT and by a factor between 1.1-2.3 for PCBM compared to the pure materials. For P3HT, degradation is resolved spatially with scanning transmission X-ray microscopy and the photo degradation process is found to be intrinsically homogeneous on the nano meter scale.

Introduction

With the improving performance reported for polymer solar cells (PSC),[1,2] the importance of increasing the operational lifetime at the device level becomes central for the realization of OPV as a scaled commercially available energy technology.[3,4] When exposed to sunlight and components in the ambient atmosphere such as water and oxygen, a number of effects occur in parallel by which the overall device performance decreases. Extensive work has been directed towards understanding these degradation mechanisms and developing new materials and geometries that can increase device lifetime.[3,5,6] Hereby, device lifetime has been observed to increase from days to months and years in recent years, and lifetimes in the range of 1-2 years are now reached with the range of 3-5 years being realistic in the near future.[7,8]

Conventionally, the device stability is assessed by exposing the functioning device to simulated sunlight while measuring the electrical performance through IV-characterization.[8,9] Whereas this approach provides a measure of the operational stability, it is a macroscopic method that gives no insight or explanations for the failure in terms of degradation mechanisms or failure mode. Whereas a trial-and-error approach can be followed by processing solar cells of e.g. different polymers or architectures to obtain more stable devices, a more rigorous approach is to study the intrinsic stability of the individual components under certain sets of conditions and thereby chart the preponderant degradation mechanisms and failure modes. Hereby, unstable components, interfaces or contacts of the device can be identified and work can be focused on remedying these, finding alternatives or simply replacing these components with better alternatives.

One device degradation mechanism that has often been found to be dominant is the degradation of the photoactive layer, where especially bleaching of the polymer has been demonstrated to be a key mechanism limiting the solar cell stability mainly in the presence of oxygen. As the photoactive polymer is exposed to light and oxygen, the polymer is prone to react chemically which implies a loss of conjugation thus affecting both light absorption, charge transport and charge collection efficiency. By monitoring the gradual photo bleaching of a large range of polymers when exposed to simulated sunlight, chemically stable functional groups have been identified.[10,11] This information may be combined with chemical analysis of the degradation products as obtained from infra-red spectroscopy by which the degradation mechanisms responsible for the polymer bleaching can be elucidated.[12–14]

The above described techniques address the photoactive layer on a macroscopic level. Other experiments have indirectly mapped degradation on the microscopic level for chemical

structures. A recent experiment mapped photocurrent and quantum efficiency for chemical structures that form 10-100 micron domains with lower EQE during degradation.[15] Although such methodologies allows for mapping degradation, they involve complete devices and results are often subject to influence by electrodes and barrier layers rather than the degradation of the active layer itself.

Other methods useful for degradation mapping of PSC materials are fluorescent microscopy and Time Of Flight Secondary Ion Mass Spectroscopy (TOF-SIMS).[16] These methods have been used to map degradation in C60/C12-PSV (Poly(didodecylstilbenevinylene)) devices, where diffusion of oxygen was tracked through pinholes in the aluminum cathode into the active layer.[17] TOF-SIMS allows tracking of elements entering the PSC materials, but has no sensitivity to other chemical changes. Fluorescent microscopy requires change in emitted fluorescence during degradation, and can normally only separate between degraded and undegraded regions, but cannot asses the level of degradation in a quantitative manner.

Compared to the previous mentioned methods, Scanning Transmission X-ray Microscopy, (STXM), can provide direct mapping of degradation. STXM has recently been applied to the field of PSCs, as this technique combines energy and nano-meter spatial resolution (Near-edge X-ray Absorption Fine Structure - NEXAFS) allowing for microscopy and chemical analysis in parallel. With this technique, imaging of the features can combined with modeling give a resolution down to 10 nm.[18] Furthermore, properties such as the molecular orientation[19,20] and the evolution of domains[21] over time have been directly imaged. Finally, the spectral information allows for quantifying the ratio of different components in the film by which *composition maps* can be obtained. Following these approaches composition maps have been demonstrated for the poly(phenylenevinylene) MDMO-PPV blended with phenyl-C_{60} butyric acid methyl ester ($PC_{60}BM$)[22] and poly-(3-hexyl-thiophene) (P3HT) blended with $PC_{60}BM$,[21,23] where the NEXAFS spectrum of the blend is fitted as a linear combination of the NEXAFS spectra of the individual components. Only limited work has been performed on the topic of degradation with STXM. The effect of degradation on the NEXAFS absorption of conjugated polymers by either *in situ* X-ray[24,25] has been reported, where pronounced effects were observed for the polymer (P3HT).

In this paper we show that the approach for obtaining linear combinations of the NEXAFS spectra of the individual components as demonstrated for P3HT and $PC_{60}BM$ can be applied for 5 other fullerene derivatives C60, C70, $PC_{70}BM$, bis$PC_{60}BM$ and ICBA (for systematic names see experimental). Additionally, by combining the NEXAFS spectra of P3HT and $PC_{60}BM$ at different degradation levels, it is possible to identify the individual degradation states of P3HT and $PC_{60}BM$ in blends. We extend the method to spatial mapping of degradation in P3HT through STXM measurements.

Results

The method we use to treat the data can be outlined as follows: Spectra of degraded blend films are compared to measured reference spectra, and the similarity is quantified. This allows us to find the state of unknown samples based on the known state of the reference samples. For absorption data the method can be extended to linear combinations due to Lambert-Beers law (see also supporting information). Thus, the state of material mixtures can be determined based on the known states of the pure components – which in most cases are easier to understand and control.

The essence of the method is to fit a spectrum with a reference spectrum (or a linear combination of multiple reference spectra) and measure the goodness of fit by reduced chi-square (for more detail see experimental section). The method falls between composition mapping,[21,23,26] which only require measurements at a few selected energies and traditional peak fitting which needs complete spectra with high energy resolution. This method only needs enough data points to perform meaningful fitting, but measured for multiple reference samples in different states since the method only determines the closest matching reference.

To check the robustness and validity of the method, we have conducted a small side study with P3HT and various fullerenes (see supporting information). We find that for differences in reduced chi-square greater than 0.1 we are able to determine the correct chemical composition.

For photo degraded P3HT-PCBM blends we use the outlined method to assign individual degradation levels to P3HT and PCBM in the blend. The degradation nomenclature is based on photo absorbance for visible light (400 – 600 nm wavelength) where T100 represent pristine material and T80 that 80% absorption is retained, relative to the pristine state. **Figure 1** shows the NEXAFS spectra of degraded P3HT, $PC_{60}BM$ and P3HT-$PC_{60}BM$ blends. For all degradation processes, the peak positions shift to higher energies as a function of photo degradation. For P3HT the spectral differences are small between T60, T80 and T100 compared to T20. $PC_{60}BM$ shows a gradual blue shift of the first two peaks and a reversal of weight between first and third peak as a function of photo degradation. The blend spectra combine the features of P3HT and $PC_{60}BM$. The T100 blend spectrum resembles a linear combination of $PC_{60}BM$ T100 and P3HT T100. The spectrum of the most degraded blend, T40, resembles the $PC_{60}BM$ T60 spectrum. Note that the two different T60 blend spectra come from the same film but different positions.

Each blend spectrum has been assigned degradation steps of P3HT and $PC_{60}BM$ based on the best linear combination of P3HT and $PC_{60}BM$ spectra. The range in P3HT degradation

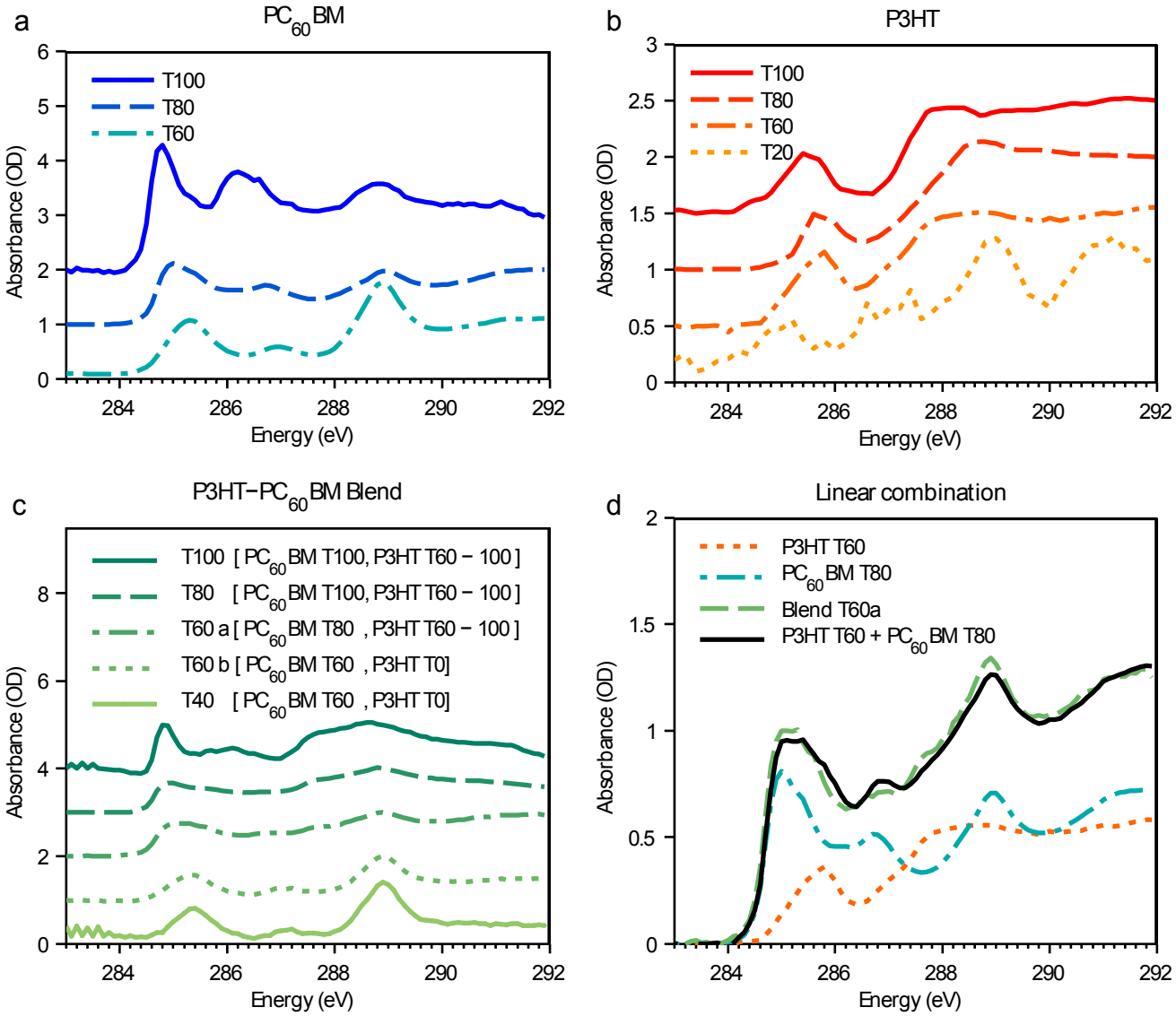

Figure 1. NEXAFS spectra for pristine and degraded (a) $PC_{60}BM$, (b) P3HT and (c) P3HT-$PC_{60}BM$ blends (1:1) in the 283 – 292 eV range. For the blends, the degradation states of the components are shown in the legend. These degradation steps have been found as the most likely linear combinations of degraded P3HT and $PC_{60}BM$ spectra - an example is shown for blend T60a in figure (d). The most likely degradation state is found by the lowest reduced chi square. The ranges in P3HT indicate regions of intervals with similar reduced chi square values.

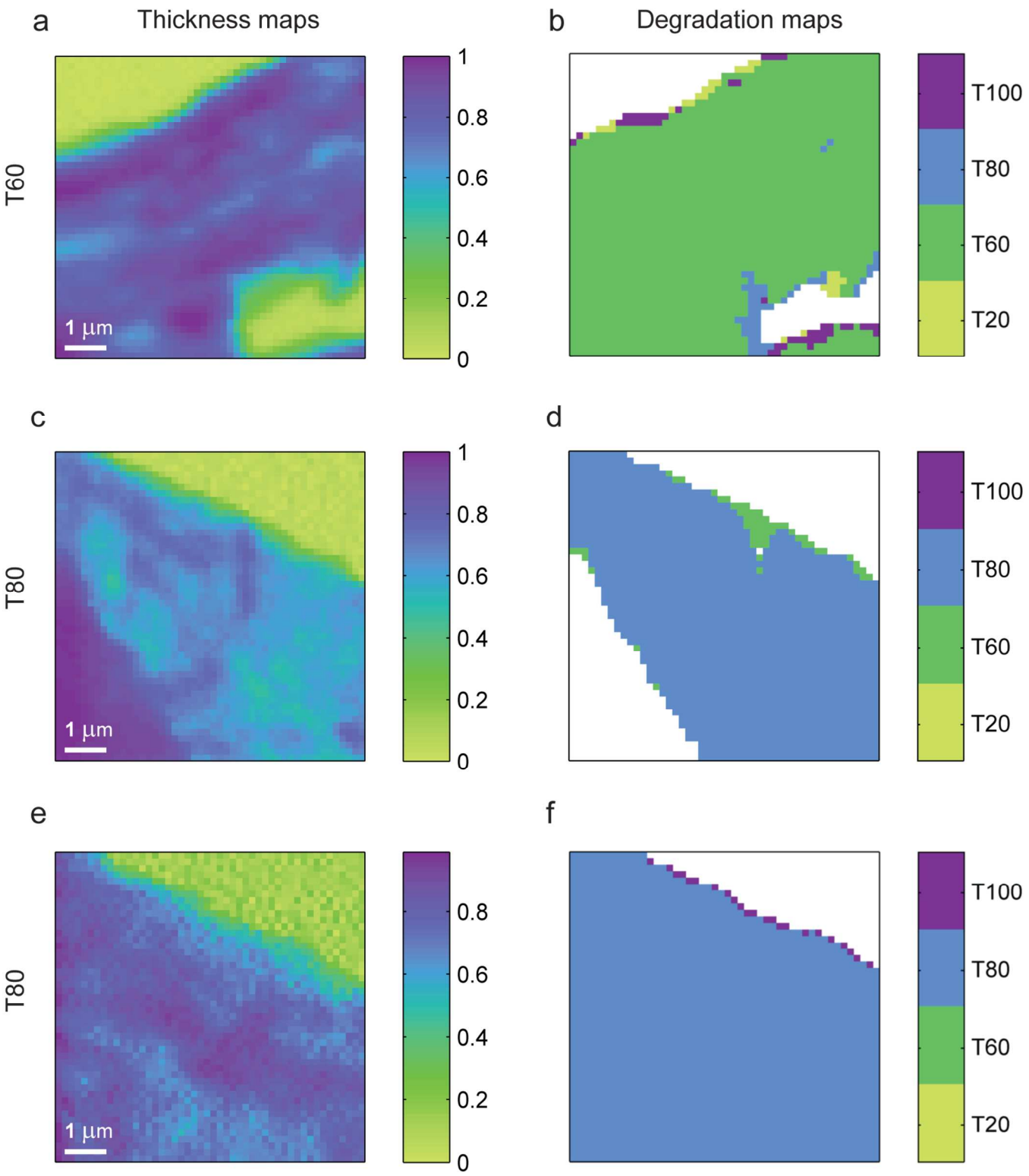

Figure 2. (a, c, e) Relative thickness of P3HT samples from STXM maps at 286 eV. The variation in thickness is a product of the fabrication method (scraped off glass substrates). (b, d, f) Degradation step found from energy resolved STXM maps. The degradation steps were assigned point by point by fitting the different P3HT reference spectra and choosing the reference with the lowest reduced chi square. Thin areas with no sample and thick areas with no photon penetration are colored white in the degradation maps (see also supporting information). (a-b) P3HT degraded to T60 level. (c-f) P3HT degraded to T80 level. For pristine P3HT (T100) see supporting information.

indicates fits where the difference in reduced chi square is less than 0.1 (as established in our test of robustness for the method). P3HT is denoted T0 in one T60 blend and the T40 blend as it is not assigned any weight in the fit i.e. the P3HT spectrum does not contribute significantly to the blend spectrum.

Figure 2 is based on energy resolved STXM and shows spatial thickness maps of P3HT in different degradation states and their associated degradation maps. Each P3HT STXM data set is fitted by the 4 NEXAFS reference degradation spectra of P3HT (T100, T80, T60, T20). Each point in an energy resolved STXM map contains a whole NEXAFS spectrum and the degradation state is found as the best fit among the reference spectra. By assigning a degradation step to each point we produce the spatial degradation maps shown in figure 2. Seen on the T60 and T80 maps the contrast goes down to pixel level (1 pixel equals 159 nm) which is also the spatial resolution since the beam diameter is smaller (31 nm). The degradation maps show largely homogeneous degradation except a few pixel sized regions in T60 and T80 in addition to all the edge regions. At the edge it is likely that the signal will partially be from the sample and partially the direct beam. The edge values therefore have low validity.

Discussion

We report the spectra of P3HT, $PC_{60}BM$ and P3HT-$PC_{60}BM$ blends degraded under controlled conditions. For $PC_{60}BM$, the absorption peaks shift to higher energies and the relative peak height is changed in the degradation process. Recent DFT calculations have determined the contribution of individual carbon elements to the $PC_{60}BM$ NEXAFS spectrum.[27] From the calculations we see that the contribution to the spectra at the lowest energies in the first peak comes from the carbon atoms in the fullerene cage. If some of these cage atoms are oxidized, the first peak will be shifted to higher energy. Furthermore, the peak near 289 eV increases in relative intensity compared to the first peak. The calculations show that the side chain of $PC_{60}BM$ mainly contributes to the peak near 289 eV, thereby indicating that the side chain is unchanged whereas the carbon cage oxidizes. This interpretation of $PC_{60}BM$ degradation through oxidation of the carbon cage is supported by MALDI-TOF studies.[28]

The P3HT spectra show less pronounced differences than $PC_{60}BM$. The T60-T100 spectra are very similar with a drastically changed spectrum for T20. The noise in the T20 pattern arises due to low X-ray absorption at the very degraded state. The similarities in the first P3HT spectra make it difficult to extract information regarding the P3HT degradation pathway. When determining the componentwise degradation in P3HT-PCBM blends, the similar spectra contribute to the ambiguity in the assessed degradation state.

The method of linear fitting reference spectra is general and can be used to track the degradation behavior in any blended material. For the P3HT-$PC_{60}BM$ blend we see that $PC_{60}BM$ degrade at a slower rate than P3HT – similar to the pure materials where $PC_{60}BM$ also endure longer exposures than P3HT before reaching the same degradation level.[10]

The contact between the two materials improves the stability of both. In our experiment it can be quantified through the degradation rates. The degradation rates of pure P3HT and PCBM have previously been reported as of 2.5%/hour for P3HT and 0.36%/hour for $PC_{60}BM$.[10] With our new measurements we can estimate the degradation rates of the materials within blend by combining the results in figure 1 with the known exposure times (see supporting information).

Assuming that P3HT reaches T0 when the blend reaches T60 the degradation rate of P3HT goes from 2.5%/hour to 0.82%/hour – a decrease to 1/3 of the original degradation rate. For $PC_{60}BM$ the decrease is somewhat lower with an original rate of 0.36%/hour and a rate in the blend between 0.16%/hour and 0.33%/hour (see figure 1 where $PC_{60}BM$ for the T60 blend samples are either T60 or T80). This corresponds to a decreased degradation rate between a factor of 1.1 to 2.3 for $PC_{60}BM$.

The decrease in the P3HT degradation rates have been conjectured to be caused by $PC_{60}BM$ quenching the excited state of P3HT.[28] For $PC_{60}BM$ the reduction in degradation rate might arise because the flow of electrons fills up vacant spaces in the homo level thereby reducing the oxidation rate. For the P3HT-$PC_{60}BM$ blends, P3HT remains the fastest degraded component and it therefore remains most important to understand the P3HT degradation process.

By using STXM, the developed method for NEXAFS spectra can map degradation spatially. We demonstrate this for pure P3HT to probe the intrinsic behavior in the degradation process. It removes any heterogeneity present in material blends and leaves us with a pure P3HT signal - removing the ambiguity in P3HT degradation we have in the P3HT-$PC_{60}BM$ blends. Through the STXM mapping of P3HT we provide the first nano scale maps of degradation in a PSC relevant polymer. The spatial maps reveal that P3HT degrade largely homogeneously at the nano scale. It indicates that polymer degradation is an evenly distributed process with no observed cooperative effects e.g. no domain growth of early degraded regions. Our method show a few domains near the resolution limit, so domain formation below the 100 nm is a possibility. There might be surface dependencies in the degradation process like oxygen diffusion, but our experiment shows that in ambient atmosphere the degradation is intrinsically homogeneous, even with thickness variation in the samples e.g. P3HT T60 in figure 2. Our results imply that the reported domain wise degradation for whole devices,[15,17] are not an intrinsic behavior in the active layer. The domain wise degradation would instead predominantly be regulated by heterogeneities in the barrier and anode/cathode layers that limit the access of oxygen and water.

Experimental

Regio-regular P3HT (Regio-regularity 91.7 %, M_n = 28.8 kDa) was obtained from Rieke Metals (Batch PTL 10-87), $PC_{60}BM$, bisPCBM (Bis(1-[3-(methoxycarbonyl)propyl]-1-phenyl)-[6.6]C62), and $PC_{70}BM$ ([6,6]-phenyl C70 butyric acid methyl-

ester) from Solenne, C60 (C60-Ih)[5,6]fullerene) and C70 (C70-Ih)[5,6]fullerene) from Aldrich, and ICBA (1',1'',4',4''-tetrahydrodi[1,4]methanonaphthaleno[5,6]fullerene-C60) from Plextronics.

Controlled Photo Degradation

All blends were processed from chlorobenzene in ratios of 1:1. Approximately 50 nm films were obtained by spin coating onto silicon nitride membranes obtained from Silson (membrane area 1 x 1 mm, thickness 100 nm). Pure P3HT samples were prepared by spin coating and photo degrading on glass. Degradation under simulated sunlight was performed with an unfiltered Osram 1200 W HMI lamp with a light intensity of 0.1 W/cm^2 at 30°C in ambient atmosphere with a light spectrum close to AM1.5G. The degradation state of the films was obtained from the gradual decrease of UV-vis absorption as described by Tromholt et al.[10] T100 indicate pristine material and T80 that 80% of the pristine photo absorbance is left in the wave length interval 400 – 600 nm.

Sample Preparation for NEXAFS experiments

Samples spin cast on silicon nitride membranes could be used directly for NEXAFS experiments (the reason why this preparation was preferred). The pure P3HT samples spin cast on glass were scraped off with a scalpel and put on transmission electron microscopy copper grids. A floating off scheme was first tried but, it was observed that the photo degraded films wrinkled and disintegrated into pieces when released from the substrate. Floating of the films were thus not deemed suitable for studying the film morphology, whereas it was conjectured that scraping off were more likely to preserve the film morphology.

STXM and NEXAFS Experiments

STXM and NEXAFS measurements were recorded at the synchrotron facility BESSY II in Berlin, Germany, at the beamline UE46-PGM2. All samples were observed in the MAXYMUS STXM end station under high vacuum at the carbon edge (282-292 eV, 1 eV resolution). The short energy range was chosen to minimize the exposure, so little or no uncontrolled degradation would occur due to the X-ray dose. In addition the beam was defocused to a diameter of (31 nm). In most experiments, the X-rays were detected by a photomultiplier tube, but the pure P3HT sample data were acquired with a photo avalanche diode. The spectra in the two experiments have been energy calibrated by the pristine P3HT absorption peaks. When measuring samples on silicon nitride membranes, the direct beam was measured in separate measurements without sample, since the whole membranes were covered with material. This is not ideal from a spectroscopy point of view, but we deemed it more important to conserve the morphology of the samples by avoiding transfer of the films after the photo degradation process.

Data Treatment of NEXAFS and STXM Data

All data were converted to optical density using the measured sample and pure beam intensity, and then normalized to 0 pre-edge and 1 post-edge similar to the procedure by Dhez et al.[29] The measured visual absorbance were related to NEXAFS spectra of the samples and these spectra were used as a reference spectra for the various states of the materials (shown in figure 1). For each P3HT-PCBM blend spectrum we fitted all linear combinations of pure P3HT and PCBM reference spectra and estimated the best fits by the reduced chi square (shown in supporting information). Component-wise degradation was estimated based on the best fits. A similar procedure was used to generate 2D degradation maps of P3HT. Energy resolved STXM data was converted to NEXAFS spectra for each point e.g. a 4x4 point STXM scan would result in 16 individual NEXAFS spectra. Each NEXAFS spectrum was fitted by the 4 P3HT reference spectra and assigned degradation state based on the best fit. Thin regions with no P3HT and thick regions with too high absorbance were removed since they could not provide valid P3HT NEXAFS spectra as described in the supporting information.

Conclusions

We explore photo degradation in ambient atmosphere for PSC materials using soft X-ray absorption microscopy. For P3HT-fullerene blends we demonstrate that individual components/degradation states can be found from linear combinations of spectra from pure materials/degradation states. This is done by finding the linear combination with the lowest reduced chi-square**.** We present the first reported NEXAFS spectra of degraded P3HT and $PC_{60}BM$, which support that $PC_{60}BM$ degrades through oxidation of the carbon cage. For P3HT-$PC_{60}BM$ blends we find that P3HT degrades faster than $PC_{60}BM$ in the blend material, but both materials reduce their degradation rate when mixed. For P3HT, the degradation rate drops by a factor of 3 and for $PC_{60}BM$ the drop is between a factor of 1.1-2.3. Finally, we demonstrate that STXM can be used to produce nano scale degradation maps of P3HT. We find that P3HT degradation is intrinsically a homogeneous process, and that the previously observed degraded domains in whole devices are effects of inhomogeneity in the barrier or electrode layers.

Acknowledgements

We gratefully acknowledge financial support from The Danish Council for Strategic Research through the WAPART project, and from The Danish Council for Independent Research | Natural Sciences, through the DANSCATT grant. We also express our gratitude to Michael Bechtel, for kind assistance during the experiments with the STXM at MAXYMUS, BESSY II, by the MPI for intelligent systems, department Schütz.

Notes and references

[a] Department of Energy Conversion and Storage, Technical University of Denmark, Frederiksborgvej 399, 4000 Roskilde, Denmark.
[b] Max Planck Institute for Intelligent Systems, Heisenbergstr. 3, 70569 Stuttgart, Germany.

† Electronic Supplementary Information (ESI) available: Contains derivation of linear combination of optical density from lambert-beers law, full chi square tables fits to blend P3HT-$PC_{60}BM$, NEXAFS data for fullerenes presented in table 1, and the degradation map of P3HT T100. See DOI: 10.1039/b000000x/

1. C. Small, S. Chen, J. Subbiah, C. Amb, S. Tsang, T. Lai, J. Reynolds, and F. So, *Nat. Photonics*, 2011, 1–6.

2. J. You, L. Dou, K. Yoshimura, T. Kato, K. Ohya, T. Moriarty, K. Emery, C.-C. Chen, J. Gao, G. Li, and Y. Yang, *Nat. Commun.*, 2013, **4**, 1446.

3. M. Jørgensen, K. Norrman, S. A. Gevorgyan, T. Tromholt, B. Andreasen, and F. C. Krebs, *Adv. Mater.*, 2012, **24**, 580–612.

4. M. O. Reese, S. A. Gevorgyan, M. Jørgensen, E. Bundgaard, S. R. Kurtz, D. S. Ginley, D. C. Olson, M. T. Lloyd, P. Morvillo, E. A. Katz, A. Elschner, O. Haillant, T. R. Currier, V. Shrotriya, M. Hermenau, M. Riede, K. R. Kirov, G. Trimmel, T. Rath, O. Inganäs, F. Zhang, M. Andersson, K. Tvingstedt, M. Lira-Cantu, D. Laird, C. McGuiness, S. (Jimmy) Gowrisanker, M. Pannone, M. Xiao, J. Hauch, R. Steim, D. M. DeLongchamp, R. Rösch, H. Hoppe, N. Espinosa, A. Urbina, G. Yaman-Uzunoglu, J.-B. Bonekamp, A. J. J. M. van Breemen, C. Girotto, E. Voroshazi, and F. C. Krebs, *Sol. Energy Mater. Sol. Cells*, 2011, **95**, 1253–1267.

5. M. Lira-Cantu, D. M. Tanenbaum, K. Norrman, E. Voroshazi, M. Hermenau, M. T. Lloyd, G. Teran-Escobar, Y. Galagan, B. Zimmermann, M. Hosel, H. F. Dam, M. Jorgensen, S. Gevorgyan, L. Lutsen, D. Vanderzande, H. Hoppe, R. Roesch, U. Wuerfel, R. Andriessen, A. Rivaton, G. Y. Uzunoglu, D. Germack, B. Andreasen, M. V Madsen, E. Bundgaard, and F. C. Krebs, in *RELIABILITY OF PHOTOVOLTAIC CELLS, MODULES, COMPONENTS, AND SYSTEMS V*, ed. Dhere, NG and Wohlgemuth, JH, 2012, vol. 8472.

6. P. Favia, E. Voroshazi, P. Heremans, and H. Bender, *J. Mater. Sci.*, 2012, **48**, 2908–2919.

7. C. J. Brabec, S. Gowrisanker, J. J. M. Halls, D. Laird, S. Jia, and S. P. Williams, *Adv. Mater.*, 2010, **22**, 3839–56.

8. C. H. Peters, I. T. Sachs-Quintana, J. P. Kastrop, S. Beaupré, M. Leclerc, and M. D. McGehee, *Adv. Energy Mater.*, 2011, **1**, 491–494.

9. S. A. Gevorgyan, A. J. Medford, E. Bundgaard, S. B. Sapkota, H.-F. Schleiermacher, B. Zimmermann, U. Würfel, A. Chafiq, M. Lira-Cantu, T. Swonke, M. Wagner, C. J. Brabec, O. Haillant, E. Voroshazi, T. Aernouts, R. Steim, J. A. Hauch, A. Elschner, M. Pannone, M. Xiao, A. Langzettel, D. Laird, M. T. Lloyd, T. Rath, E. Maier, G. Trimmel, M. Hermenau, T. Menke, K. Leo, R. Rösch, M. Seeland, H. Hoppe, T. J. Nagle, K. B. Burke, C. J. Fell, D. Vak, T. B. Singh, S. E. Watkins, Y. Galagan, A. Manor, E. A. Katz, T. Kim, K. Kim, P. M. Sommeling, W. J. H. Verhees, S. C. Veenstra, M. Riede, M. Greyson Christoforo, T. Currier, V. Shrotriya, G. Schwartz, and F. C. Krebs, *Sol. Energy Mater. Sol. Cells*, 2011, **95**, 1398–1416.

10. T. Tromholt, M. V. Madsen, J. E. Carlé, M. Helgesen, and F. C. Krebs, *J. Mater. Chem.*, 2012, **22**, 7592.

11. M. Manceau, E. Bundgaard, J. Eggert Carlé, O. Hagemann, M. Helgesen, R. Søndergaard, M. Jørgensen, and F. C. Krebs, *J. Mater. Chem.*, 2011, **21**, 4132–4141.

12. M. Manceau, J. Gaume, A. Rivaton, and J. Gardette, *Thin Solid Films*, 2010, **518**, 7113–7118.

13. A. Rivaton, S. Chambon, M. Manceau, J.-L. Gardette, N. Lemaître, and S. Guillerez, *Polym. Degrad. Stab.*, 2010, **95**, 278–284.

14. M. Manceau, A. Rivaton, J.-L. Gardette, S. Guillerez, and N. Lemaître, *Polym. Degrad. Stab.*, 2009, **94**, 898–907.

15. K. Feron, T. J. Nagle, L. J. Rozanski, B. B. Gong, and C. J. Fell, *Sol. Energy Mater. Sol. Cells*, 2013, **109**, 169–177.

16. B. Andreasen, D. M. Tanenbaum, M. Hermenau, E. Voroshazi, M. T. Lloyd, Y. Galagan, B. Zimmernann, S. Kudret, W. Maes, L. Lutsen, D. Vanderzande, U. Würfel, R. Andriessen, R. Rösch, H. Hoppe, G. Teran-Escobar, M. Lira-Cantu, A. Rivaton, G. Y. Uzunoğlu, D. S. Germack, M. Hösel, H. F. Dam, M. Jørgensen, S. A. Gevorgyan, M. V Madsen, E. Bundgaard, F. C. Krebs, and K. Norrman, *Phys. Chem. Chem. Phys.*, 2012, **14**, 11780–99.

17. K. Norrman, N. B. Larsen, and F. C. Krebs, *Sol. Energy Mater. Sol. Cells*, 2006, **90**, 2793–2814.

18. K. B. Burke, A. J. Stapleton, B. Vaughan, X. Zhou, A. L. D. Kilcoyne, W. J. Belcher, and P. C. Dastoor, *Nanotechnology*, 2011, **22**, 265710.

19. B. Watts, T. Schuettfort, and C. R. McNeill, *Adv. Funct. Mater.*, 2011, **21**, 1122–1131.

20. D. S. Germack, C. K. Chan, B. H. Hamadani, L. J. Richter, D. A. Fischer, D. J. Gundlach, and D. M. DeLongchamp, *Appl. Phys. Lett.*, 2009, **94**, 233303.

21. B. Watts, W. J. Belcher, L. Thomsen, H. Ade, and P. C. Dastoor, *Macromolecules*, 2009, **42**, 8392–8397.

22. C. R. McNeill, B. Watts, L. Thomsen, W. J. Belcher, A. L. D. Kilcoyne, N. C. Greenham, and P. C. Dastoor, *Small*, 2006, **2**, 1432–5.

23. K. Burke, W. Belcher, and L. Thomsen, *Macromolecules*, 2009, **42**, 3098–3103.

24. H. Ahn, D. Oblas, and J. Whitten, *Macromolecules*, 2004, **37**, 3381–3387.

25. L.-L. Chua, M. Dipankar, S. Sivaramakrishnan, X. Gao, D. Qi, A. T. S. Wee, and P. K. H. Ho, *Langmuir*, 2006, **22**, 8587–94.

26. B. A. Collins and H. Ade, *J. Electron Spectros. Relat. Phenomena*, 2012, **185**, 119–128.

27. I. E. Brumboiu, A. S. Anselmo, B. Brena, A. Dzwilewski, K. Svensson, and E. Moons, *Chem. Phys. Lett.*, 2013, **568-569**, 130–134.

28. M. O. Reese, A. M. Nardes, B. L. Rupert, R. E. Larsen, D. C. Olson, M. T. Lloyd, S. E. Shaheen, D. S. Ginley, G. Rumbles, and N. Kopidakis, *Adv. Funct. Mater.*, 2010, **20**, 3476–3483.

29. O. Dhez, H. Ade, and S. G. Urquhart, *J. Electron Spectros. Relat. Phenomena*, 2003, **128**, 85–96.